Solid Freeform Fabrication 2024: Proceedings of the 35th Annual International Solid Freeform Fabrication Symposium – An Additive Manufacturing Conference
Reviewed Paper

STATISTICAL PROCESS CONTROL FOR WAAM FOR PRODUCTIVITY AND QUALITY IMPROVEMENTS

Austen Thien* †, Christopher Saldana*
*George W. Woodruff School of Mechanical Engineering
Georgia Institute of Technology
801 Ferst Drive, Atlanta, GA, 30332, USA
†athien6@gatech.edu

Keywords: wire-arc additive manufacturing, closed-loop control, statistical process control

Abstract

Wire-arc additive manufacturing (WAAM) is a wire-fed welding-based metal additive manufacturing process where the thermal management greatly influences build quality. The interlayer dwell time is a critical parameter that determines the process condition stability, the geometric uniformity and the overall production time of the build. Thus, control strategies are needed for the WAAM process to produce stable geometry and deposition conditions while minimizing production times. In this study, a closed-loop control technique uses cumulative summation (CUSUM) to detect in-situ statistical deviations of contact tip to workpiece distance (CTWD) and current data caused by short interlayer dwell times and then implements corrective process parameters to compensate. This CUSUM control loop is applied to single-bead 20-layer WAAM builds using mild steel (ER70S-6) material. The effects of input data stream choice and corrective parameter value on the controller performance are determined by evaluating production metrics, statistical distribution of process data, and response time.

Introduction

Wire-arc additive manufacturing (WAAM) is a metal additive manufacturing process that utilizes conventional welding processes to deposit material layer by layer until a near-net shape geometry is achieved. The wire feedstock of the WAAM process allows for higher production rates and larger part feature sizes than metal additive manufacturing (AM) processes that use powder feedstock [1]. As with other AM processes, there can be considerable variation in the deposited WAAM geometry due to both the layer-wise buildup of material inherent to AM processes and the large surface roughness that comes with the larger bead sizes that are possible using wire-fed AM processes [2–4]. WAAM bead morphology is dependent on both the material deposition rate and the thermal conditions of the deposition. The material deposition rate is governed by the wire feed speed (WFS) and traverse speed (TS), commonly expressed as the WFS/TS ratio [3]. While those parameters control how much material is deposited, the heat input and the cooling rate affect how that material is distributed on the deposition surface. The heat input determines how much of the previously deposited layer is remelted and fused with the material in the layer currently being deposited. The cooling rate, commonly parameterized as either interlayer dwell time or interlayer temperature, influences the surface temperature of the previously deposited layer and thus the surface tension of the material in the subsequently deposited layer [5,6]. Depending on the selection of the WAAM process parameters, the discrepancies in the individual bead geometry can

accumulate as more layers are deposited which can result in disparate bulk as-deposited part geometries [3,7–9]. In general, for a given TS, WFS combination, WAAM processes that utilize a lower interlayer dwell time/higher interlayer temperature exhibit bulk part geometries that are shorter and wider than WAAM processes that use a high interlayer dwell time/low interlayer temperature. In addition to the geometric disparities that arise from using low interlayer dwell times, there can also be considerable variations in the process conditions such as current and CTWD [8]. While the as-deposited geometry and WAAM process conditions can be stabilized by using a high interlayer dwell time as mentioned above this approach adds a considerable amount of production time, most of which is when the WAAM system is idle [2,8,10]. Additionally, in many commercially available motion systems it is not easy or possible to update the workpiece offsets and so the lower bead height caused by using a low interlayer dwell time means that the part is underbuilt and thus the target part height is never reached [8,11]. Thus, it is desirable to apply closed-loop control techniques to the WAAM process so that the production time benefits of using a low interlayer dwell time can be achieved while still maintaining target part height and minimizing any variations in WAAM process conditions.

Research in additive process control has been featured widely in literature due to the desire to correct and control the as-deposited geometry [12]. Previous work has applied a range of closed-loop control algorithms utilizing various combinations of deposition and motion control parameters in both single input single output (SISO) and multi-input multi-output (MIMO) formats. The specific configuration of the WAAM system determines the corrective control actions available from the deposition and motion control subsystem and the openness of the controller architecture determines at what frequency corrective control actions can be executed and what process variables can be used as control actions [13–22]. Open controller architectures have allowed for high frequency or continuous control, where deposition and motion parameters can be adjusted within a single layer, and controller architectures with less access are limited to low-frequency or intermittent control, where parameters are changed in between layers. The studies that have utilized intermittent control for managing defects between successive layers mostly relied on conventional iterative learning control (ILC) techniques or even updating the path plan in-situ to compensate [13,14]. Motion systems utilizing commercial machine tool controllers and G-Code are limited to intermittent control due to the capability of bi-directional communication to and from the controller being limited by design [11]. Therefore, WAAM systems using this type of motion subsystem cannot adjust their CTWD offset or TS within a deposition layer.

An important sub-set of closed-loop control is statistical process control where statistical methods are utilized to monitor and control process quality. Typically, the output of the process is monitored via a control chart that helps the user to map when statistical variations in the process output exceed predefined control limits and are thus attributed to more than just the expected common variation of the process in question [23,24]. Statistical process control techniques have been utilized in conventional welding processes to quickly detect fluctuations in single weld beads by monitoring high frequency process data when disturbances in the joints are introduced [25–27]. Previous efforts in applying statistical process control methods and control charts have been extremely limited, mostly concerning detection of contaminants in the WAAM melt pool [28–30]. The present study seeks to apply statistical process control to WAAM so that the process condition

instability stemming from the usage of shorter interlayer dwell times can be corrected, thus decreasing the overall production time while maintaining quality control of the WAAM process.

Methodology

The experimental setup used in this work consists of a Lincoln Electric PowerWave S500 power supply integrated into a Cincinnati Dart 500 3-axis CNC machine. The WAAM process uses MIG welding with short-circuit droplet transfer to deposit material. The welding torch is inserted into the spindle of the CNC with CAT40 tool holder as shown in Figure 1a below. The wire feedstock used is 1.2 mm diameter ER70S-6 mild steel and the shield gas used is 99.99% ultra high purity (UHP) argon. Current and voltage data is collected from the power supply at ~10 Hz, and the CTWD is measured at ~5 Hz via an externally mounted weld camera shown in Figure 1a. Since the Siemens 828D controller on the CNC machine does not allow for reading or writing data via commercially available machine tool automation protocols like MTConnect or OPCUA, and so a servo-actuated gear train, seen in Figure 1b below, is installed on the feed rate override knob to automate changes in the WAAM traverse speed. The servo motor is connected to an edge device that can receive motion commands based on changes in the in-situ process data. While this approach allows one to automate changing the traverse speed of the WAAM process, the feed rate override knob is only capable of discrete values for the traverse speed.

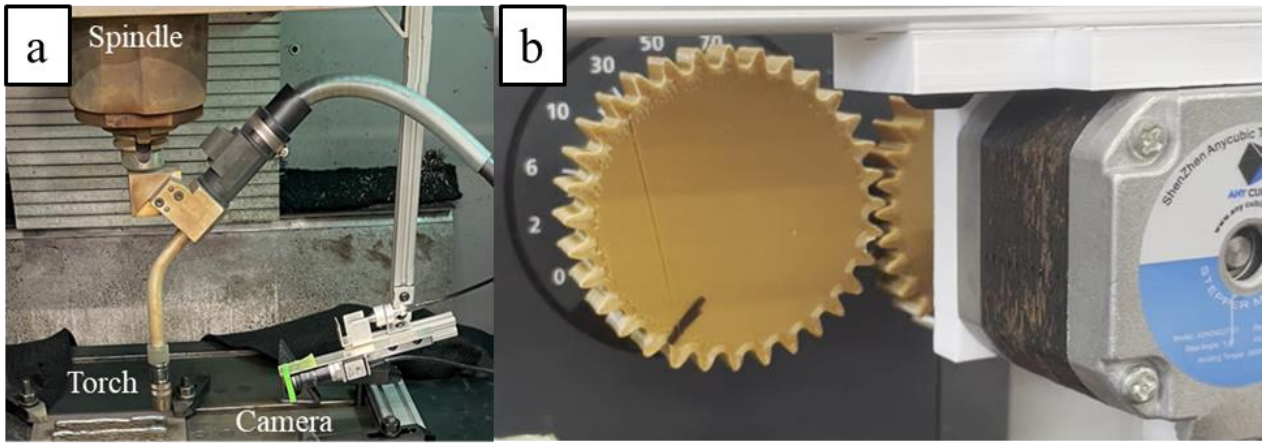

Figure 1: Retrofit-CNC WAAM Experimental Setup; a) WAAM torch and external sensor, b) servo-actuated feed rate override knob

To compensate for underbuilding caused by using a low interlayer dwell time, the appropriate parameters must be applied that cause overbuilding during the WAAM process. Earlier work by Li et al. [7], Kozamernik et al. [31] has demonstrated how reducing heat accumulation through increasing dwell time or decreasing power input can increase part height. These methods do not alter the material input rate but rather use the deposited material more efficiently to increase part height. Other studies have controlled part height by altering material input rate, such as Fathi et al. [19], Lam et al. [20], and Banerjee et al. [32] who changed the traverse speed to vary bead height, and Heralic et al. [13] and Reisgen et al. [14] who controlled the bead height by altering wire feed speed. There have also been methodologies explored by Heralic et al. [13], Reisgen et al. [14], and Scenitec et al. [17] to mitigate underbuilding by controlling and updating the CTWD

position offset after every layer, but this approach is not feasible with the WAAM system used in this study due to the configuration of the CNC controller.

From the earlier discussion about the effect of material deposition rate, heat input, and cooling rates on bead geometry, three individual compensation parameter strategies are identified: decreasing the input power, increasing the dwell time, and decreasing the traverse speed. Additionally, several strategies are implemented that use two of these parameters in tandem: combining low power with high interlayer dwell and combining low traverse speed with high interlayer dwell time. The first combination is tested to assess if decreasing the power will enhance the overbuilding phenomenon achieved by increasing the interlayer dwell time. The second combination is made because while decreasing the traverse speed increases the amount of material deposited it also increases the heat input. Thus, if the low traverse speed is used with a low interlayer dwell time, there will still be significant underbuilding. The candidate compensation parameter sets and are depicted below in Figure 2. While the wire feed speed does affect the heat and material input rates, it also changes the current used in the deposition process. This means that if the wire feed speed is altered during the deposition process the effects of underbuilding on the current, as seen in previous work by Thien et al. [8], could not be independently assessed and thus the current would not be a reliable data stream for in-situ monitoring. Therefore, the WFS is kept constant at 88.9 mm/s.

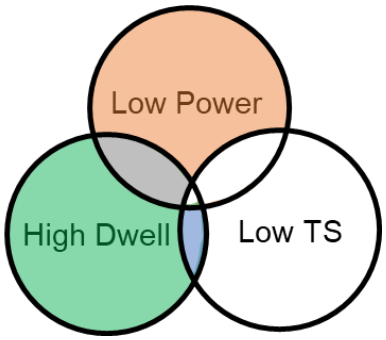

Figure 2: Over-building compensation parameter combinations

To effectively benchmark the potential of these candidate compensation parameter sets, initial closed-loop control experiments are conducted using a simplified “on-off” control strategy pictured below in Figure 3. “On-off” methods of closed loop control have only rarely applied to the WAAM process for interlayer control, as most methodologies have taken advantage of customizable or open-source motion controllers to continuously update the torch position. In the “on-off” control loop used in this work, a reference bead is first deposited and the average current and CTWD values are calculated and used as the control loop setpoint [17]. Then, the WAAM process is run using a low interlayer dwell time and the in-situ process data streams of current and CTWD are monitored until an arbitrary error threshold is exceeded. At this point the candidate compensation parameter(s) are applied until the error decreases below the threshold. This process is repeated until the deposition process is finished. The deposition geometry parameters are seen below in Table 1.

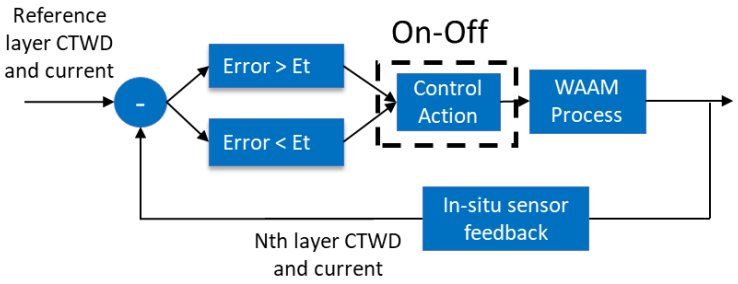

Figure 3: "On-off" control loop for compensation parameter testing

Table 1: Deposition geometry parameters

Programmed Layer Height* (mm)	Number of Layers	Expected Part Height (mm)	Deposition Bead Length (mm)
2.03	20	40.6	152.4

*After each layer is deposited, the WAAM torch increases in the Z-axis by this amount. This is programmed into the CNC controller.

The underbuilding and overbuilding deposition process parameters are seen below in Table 2, where P: power input, T_D: interlayer dwell time, UB: underbuilding, and OB: overbuilding. The selection of the overbuilding compensation traverse speed TS_{OB} and overbuilding compensation interlayer dwell time $T_{D,\,OB}$ are based on previous work [8].

Table 2: Deposition process parameters

Candidate Compensation Parameter Set	P_{UB} (kW)	TS_{UB} (mm/s)	$T_{D,UB}$ (s)	P_{OB} (kW)	TS_{OB} (mm/s)	$T_{D,OB}$ (s)
Low P	2.1	6.77	0	1.5	6.77	0
High T_D	2.1	6.77	0	2.1	6.77	60
Low P and high T_D	2.1	6.77	0	1.5	6.77	60
Low TS and high T_D	2.1	6.77	0	2.1	4.23	60

The results from the candidate compensation parameter benchmarking experiments can be seen below in Figure 4. The CTWD and current values are expressed relative to the reference CTWD and current from the first bead deposited during each deposition and are denoted as ΔCTWD and ΔCurrent. The least effective overbuilding compensation method is the low power option, as the ΔCTWD and ΔCurrent values at the end of the twenty-layer build are approximately 7 mm and -26 amps, respectively. Next the high dwell and low power/high dwell overbuilding compensation methods result in final ΔCTWD and ΔCurrent values of approximately 3 mm, -12 amps and 2 mm, -8 amps, respectively. This indicates that while the combination of low power and high dwell compensation performs better than just high dwell compensation alone, neither method can fully compensate for the underbuilding introduced during the short interlayer dwell time portions of the build. The low traverse speed/high dwell compensation method performs the best as it can consistently compensate for underbuilding and results in final ΔCTWD and ΔCurrent values of approximately -1 mm and -6 amps, respectively. Therefore, the most ideal overbuilding

compensation parameter set to use for further closed-loop experiments is the combination of low traverse speed and high dwell time. This outcome aligns with the existing knowledge of process parameter-bead morphology interactions discussed earlier as the lower traverse speed increases the amount of material being deposited and the higher interlayer dwell time decreases the surface temperature of the previously deposited layer, which decreases the degree of wetting in the material of the subsequently deposited layer. This has the combined effect of depositing beads tall enough to compensate for underbuilding. The fact that the combination of traverse speed and interlayer dwell is more effective at controlling part height than the single parameter approaches aligns well with the results of previous studies which demonstrate that using two or more WAAM process parameters is an ideal method for interlayer part height control [13,14,21,32].

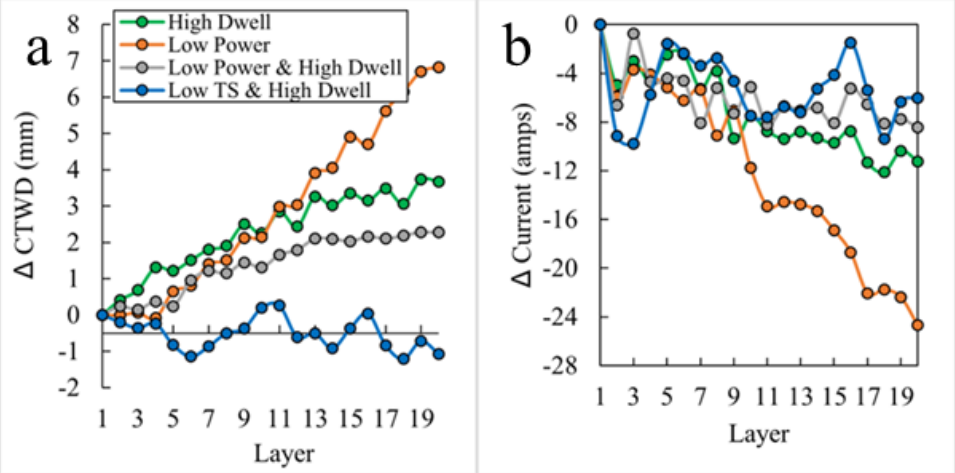

Figure 4: Initial compensation parameter closed-loop control results; a) CTWD, b) current

Once benchmarking of the candidate compensation parameter sets is completed, the most promising compensation parameter set will be used in more sophisticated statistical process control experiments. The statistical process control method used in this work is CUSUM, which stands for CUmulative SUMmation, and is a sequential analysis statistical process control technique that is used to detect small changes in the process mean relative to the expected mean of the process when it is in control [23,24,33]. The CUSUM process control algorithm utilized in this study is depicted below in Figure 5. First, the initial reference bead is deposited using the underbuilding parameters. The mean and standard deviation of both the current and CTWD are calculated from this reference bead and then used as the setpoint for the CUSUM control technique. As each layer in the WAAM process is deposited, in-situ current and CTWD process data is collected for that layer and split into several packets. The average current and CTWD value for each packet is then calculated and used as inputs to the CUSUM calculation. The packeting approach is done so that there are multiple inputs to the CUSUM value for each layer. If the CUSUM metric deviates beyond either the upper or lower control limits, then underbuilding or overbuilding compensation parameter sets are applied. This process is repeated until all twenty layers have been deposited. Thus, the CUSUM monitoring method is now applied in an “on-off” control loop, similar to the approach used by Cowan et al. [33].

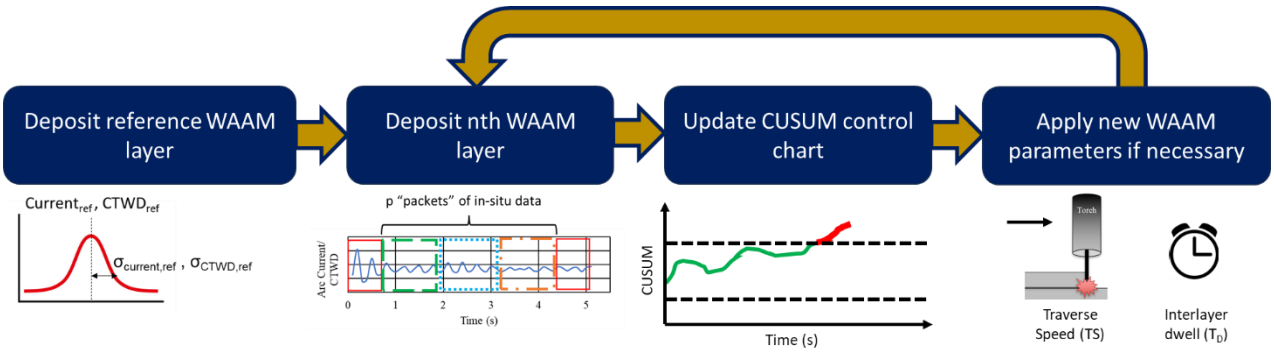

Figure 5: WAAM CUSUM process control algorithm

The mathematical formulation for the CUSUM metric is relatively straightforward and only utilizes a couple of equations. The individual packet values of current and CTWD are first used to calculate the z-statistic so that the in-situ process data can be represented as a number of standard deviations away from the reference mean:

$$Z_{current,m} = \frac{Current_{n,m} - Current_{ref}}{\sigma_{current,ref}} \quad (1)$$

$$Z_{CTWD,m} = \frac{CTWD_{n,m} - CTWD_{ref}}{\sigma_{CTWD,ref}} \quad (2)$$

Where Z: z-statistic, n: layer number, m: packet number for layer n (m = 1, 2, … p for p packets).

Next, the Z-statistic value for each packet is accumulated into the running total of the CUSUM value as shown below. To distinguish between positive and negative deviations from the reference mean, two CUSUM values are used. Additionally, a sensitivity parameter is included in the CUSUM calculation control the magnitude of the deviations that affect the CUSUM value.

$$Sh_{current,n} = \max\left(0, Sh_{current,n-1} + \left(Z_{current,m} - K\right)\right) \quad (3)$$

$$Sl_{current,n} = \max\left(0, Sl_{current,n-1} + \left(-Z_{current,m} - K\right)\right) \quad (4)$$

$$Sh_{CTWD,n} = \max\left(0, Sh_{CTWD,n-1} + \left(Z_{CTWD,m} - K\right)\right) \quad (5)$$

$$Sl_{CTWD,n} = \max\left(0, Sl_{CTWD,n-1} + \left(-Z_{CTWD,m} - K\right)\right) \quad (6)$$

Where Z: z-statistic, n: layer number, m: packet number for layer n (m = 1, 2, … p for p packets), Sh: CUSUM value related to positive deviations from the reference mean, Sl: CUSUM value related to negative deviations from the reference mean, and K: sensitivity parameter. The sensitivity parameter K is set to 0.5 based on previously developed heuristics and prior literature [23,24,33].

The control loop for the CUSUM implementation can be seen below in Figure 6 where it can be seen that the $Sh_{current,n}$, $Sl_{current,n}$, $Sh_{CTWD,n}$, and $Sl_{CTWD,n}$ parameters are continuously updated with in-situ process data from the nth layer being deposited. When these values exceed the predefined control limits, either underbuilding or overbuilding parameters are applied. Thus, the control scheme uses CUSUM monitoring in an "on-off" format, similar to other manufacturing approaches [33]. The control limit values $H_{current}$ and H_{CTWD} are set to 5 based on previously

developed heuristics and prior literature [23,24,33]. Since the process data trends for current and CTWD during underbuilding are inversely related, namely that the current decreased while the CTWD increases, the CUSUM on-off control law has been formulated to reflect this behavior.

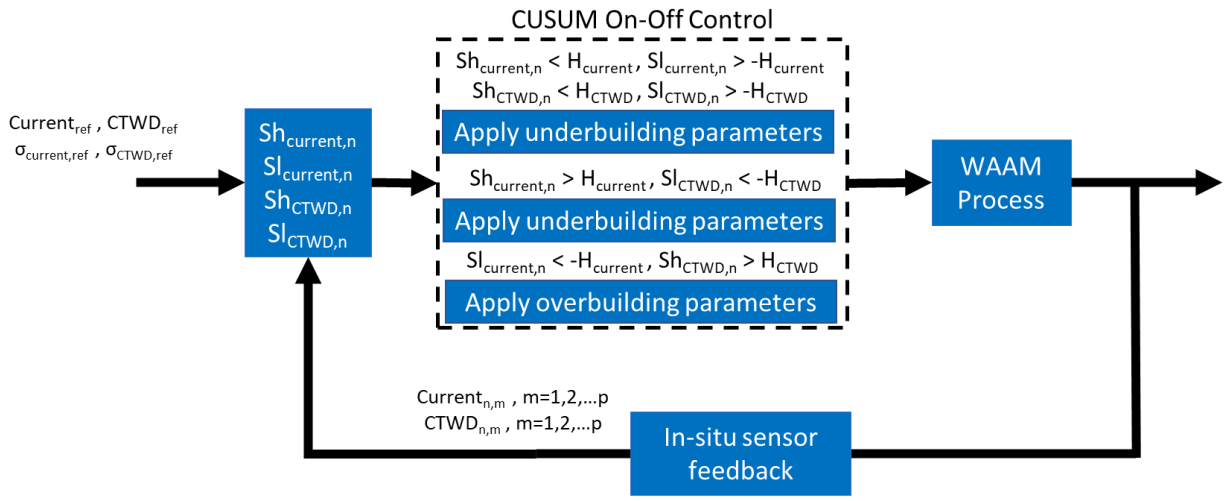

Figure 6: CUSUM control loop

The experimental factors altered in this study can be seen below in Table 3. The data types of current and CTWD are independently evaluated as inputs to the CUSUM algorithm. Additionally, the magnitude of the overbuilding compensation traverse speed TS_{OB} is altered. Since the feed rate override knob can only allow for discrete values of the traverse speed, the experimental overbuilding compensation traverse speed values are limited to 4.23, 5.08, and 5.93 mm/s. The overbuilding compensation interlayer dwell $T_{D,\,OB}$ is kept at 60 s based on heuristics developed from prior work [8].

Table 3: CUSUM experiment process parameters

CUSUM Input Data Stream	P_{UB} (kW)	TS_{UB} (mm/s)	$T_{D,UB}$ (s)	P_{OB} (kW)	TS_{OB} (mm/s)	$T_{D,OB}$ (s)
CTWD	2.1	6.77	0	2.1	5.93	60
CTWD	2.1	6.77	0	2.1	5.08	60
CTWD	2.1	6.77	0	2.1	4.23	60
Current	2.1	6.77	0	2.1	5.93	60
Current	2.1	6.77	0	2.1	5.08	60
Current	2.1	6.77	0	2.1	4.23	60

Results and Discussion

The CUSUM control charts for the experiments where CTWD is used as the input can be seen below in Figure 7 with the control action values for the interlayer dwell time and traverse speed during each build seen in Figure 8a and Figure 8b, respectively. For all values of TS_{OB} the CUSUM metric Sh_{CTWD} exceeds the control limit H_{CTWD} at beads 5-6 when the Sh_{CTWD} CUSUM value ranges from 13-17. After this point, the overbuilding compensation parameters are applied according to Table 3 above. When TS_{OB} = 4.23 mm/s there are two regions of underbuilding, from layers 1-5 and from layers 10-15, and two regions of overbuilding, from layers 6-9 and from layers 16-20. In the first region of overbuilding the Sh_{CTWD} CUSUM value spikes at approximately 30, and in the second region of overbuilding the Sh_{CTWD} CUSUM value hits a maximum of approximately 88. In the intervening region of underbuilding, the Sl_{CTWD} CUSUM value reaches a minimum of approximately -90. When TS_{OB} = 5.08 mm/s there are also two regions of underbuilding, from layers 1-4 and from layers 9-12, and two regions of overbuilding, from layers 5-8 and from layers 13-20. In the first region of overbuilding the Sh_{CTWD} CUSUM value increases to approximately 23, and in the second region of overbuilding the Sh_{CTWD} CUSUM value hits a maximum of approximately 98. In the intervening region of underbuilding, the Sl_{CTWD} CUSUM value reaches a minimum of approximately -32. When TS_{OB} = 5.93 mm/s there is one region of underbuilding from layers 1-5 and the rest of the build from layers 6-20 is using overbuilding compensation parameters where the Sh_{CTWD} CUSUM value plateaus at approximately 92 at the end of the build.

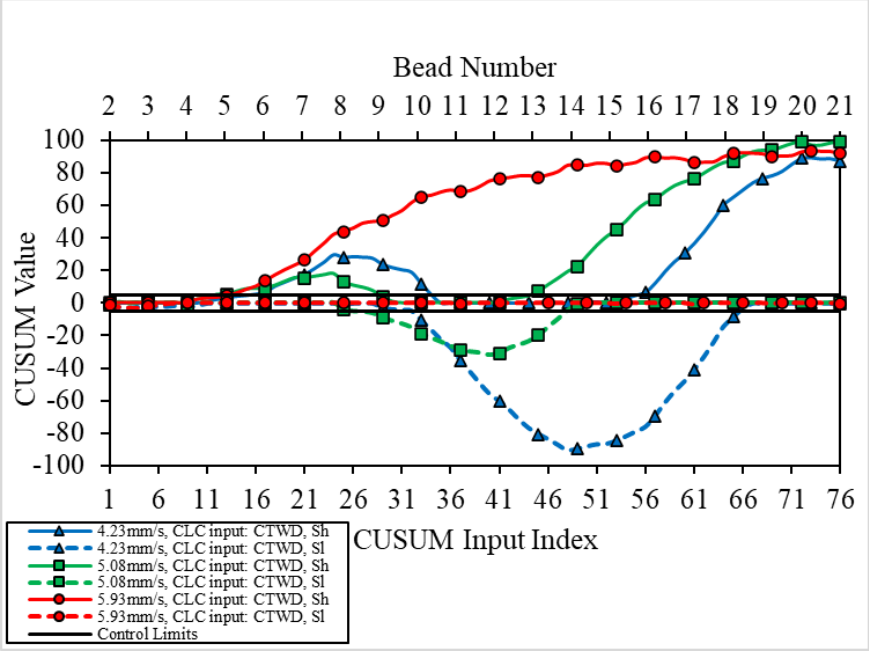

Figure 7: CUSUM control chart for CTWD input, showing positive CUSUM value (Sh) and negative CUSUM values (Sl). Lower x-axis indicates time series of inputs to CUSUM algorithm, upper x-axis indicates bead numbers of deposition process.

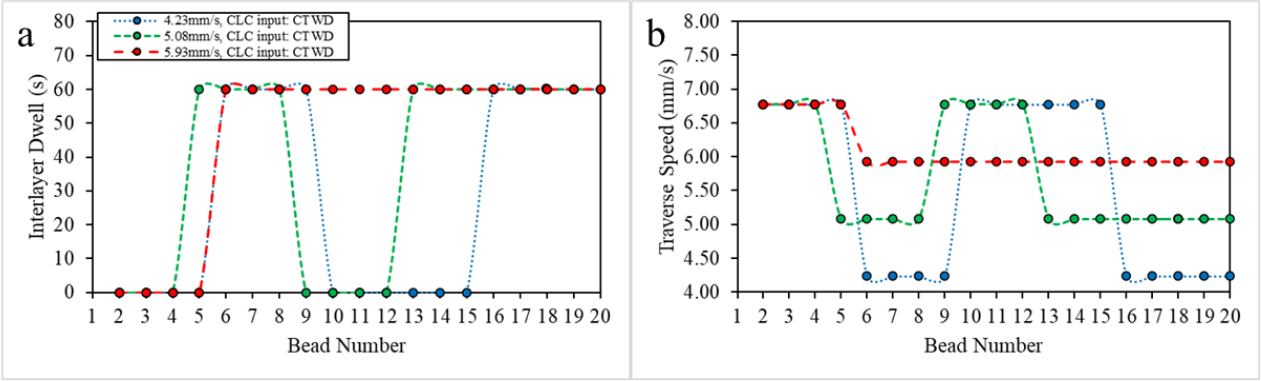

Figure 8: Control action values CTWD CUSUM input; a) interlayer dwell time, b) traverse speed

The average layer values for current and CTWD can be seen in Figure 9a and Figure 9b, respectively. For the experiment where TS_{OB} = 4.23 mm/s, the CTWD ranges from approximately -1 to 1 mm with the current ranging from approximately 167 to 175 amps. When TS_{OB} = 5.08 mm/s, the CTWD ranges from approximately -0.5 to 0.8 mm with the current ranging from approximately 168 to 176 amps. Finally, when TS_{OB} = 5.93 mm/s, the CTWD ranges from -0.18 to 0.7 mm with the current ranging from 170 to 176 amps.

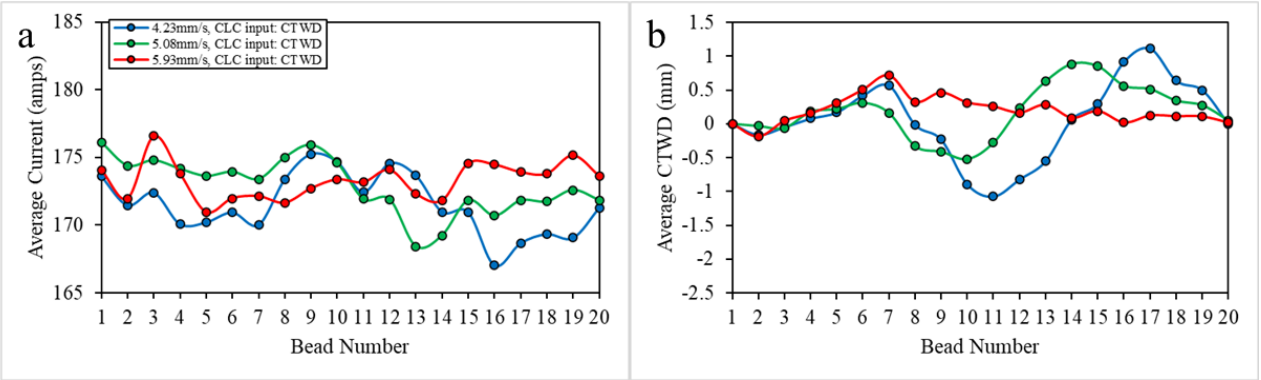

Figure 9: Bead average values for CTWD CUSUM input; a) current, b) CTWD

The local maxima and minima seen in the Sh_{CTWD} and Sl_{CTWD} CUSUM values are akin to "overshoot" in conventional closed-loop control terminology and the number of layers of each underbuilding and overbuilding region are important as they will influence the overall production time. It can be seen from the control charts in Figure 7 and the graphs of control actions in Figure 8 above that while the use of the lowest TS_{OB} = 4.23 mm/s results in 10 layers using 0s interlayer dwell time, it also results in the widest range of Sh_{CTWD} and Sl_{CTWD} CUSUM values and the widest range of average bead CTWD values. When TS_{OB} = 5.08 mm/s, the range of Sh_{CTWD} and Sl_{CTWD} CUSUM values and bead average CTWD values decreases but only 8 layers use the 0s interlayer dwell time. Lastly, when TS_{OB} = 5.93 mm/s the Sl_{CTWD} CUSUM value never exceeds the given control limit but the Sh_{CTWD} CUSUM value goes beyond the control limit for the majority of the build which causes only the first 5 layers to use the 0 s interlayer dwell time. It should also be noted that the range of average layer current values is between 6 and 8 amps.

The CUSUM control charts for the experiments where current is used as the input can be seen below in Figure 10 with the control action values for the interlayer dwell time and traverse speed during each build seen in Figure 11a and Figure 11b, respectively. For all values of TS_{OB} the CUSUM metric $Sl_{current}$ exceeds the control limit $-H_{current}$ at bead 6 when the $Sl_{current}$ CUSUM value ranges from -5 to -7. After this point, the overbuilding compensation parameters are applied according to Table 3 above. When TS_{OB} = 4.23 mm/s there are two regions of underbuilding, from layers 1-5 and from layers 15-20, and one region of overbuilding from layers 6-14. In the overbuilding region the $Sl_{current}$ CUSUM value reaches a local minimum of approximately -23. In the second region of underbuilding, the $Sh_{current}$ CUSUM value reaches a maximum of approximately 32. When TS_{OB} = 5.08 mm/s there are also two regions of underbuilding, from layers 1-5 and from layers 18-20, and one region of overbuilding from layers 6-17. In overbuilding region, the $Sl_{current}$ CUSUM value reaches a minimum of -22. In the second region of underbuilding, the $Sh_{current}$ and $Sl_{current}$ CUSUM values remain within the control limits. When TS_{OB} = 5.93 mm/s there is one region of underbuilding from layers 1-5 and the rest of the build from layers 6-20 is using overbuilding compensation parameters where the $Sl_{current}$ CUSUM value decrease linearly as the build progresses, ending at an approximate value of -45.

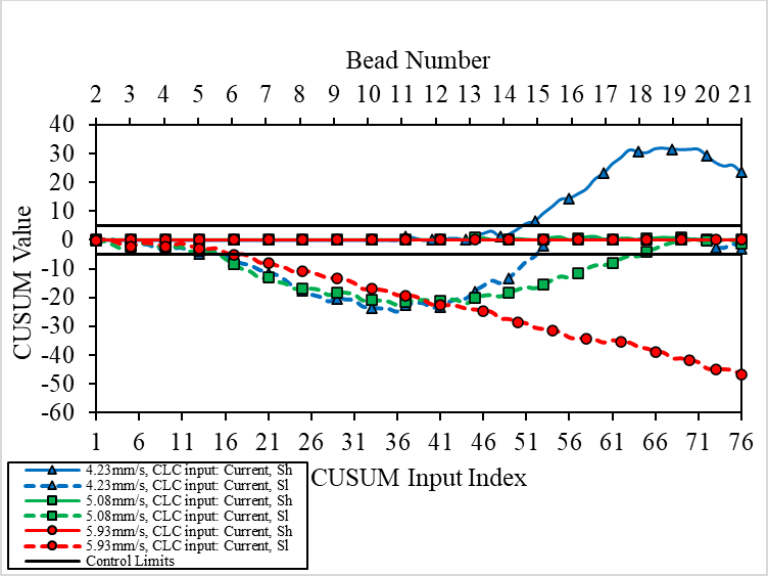

Figure 10: CUSUM control chart for current input, showing positive CUSUM value (Sh) and negative CUSUM values (Sl). Lower x-axis indicates time series of inputs to CUSUM algorithm, upper x-axis indicates bead numbers of deposition process.

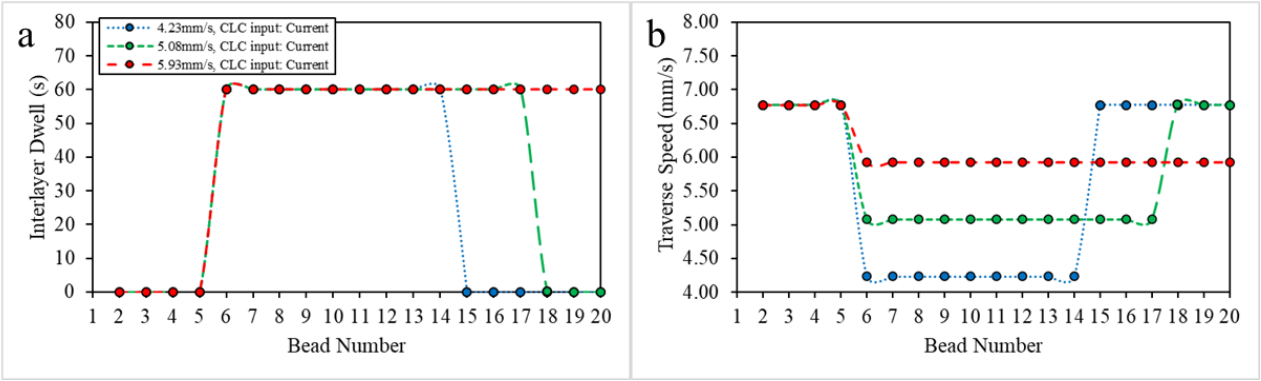

Figure 11: Control action values current CUSUM input; a) interlayer dwell time, b) traverse speed

The average layer values for current and CTWD can be seen in Figure 12a and Figure 12b, respectively. For the experiment where TS_{OB} = 4.23 mm/s, the CTWD ranges from approximately -2.25 to 0.8 mm with the corresponding current ranging from approximately 169 to 181 amps. When TS_{OB} = 5.08 mm/s, the CTWD ranges from approximately -1.2 to 0.65 mm with the current ranging from approximately 168 to 175 amps. Finally, when TS_{OB} = 5.93 mm/s, the CTWD ranges from -0.05 to 1mm with the current ranging from 169 to 173 amps.

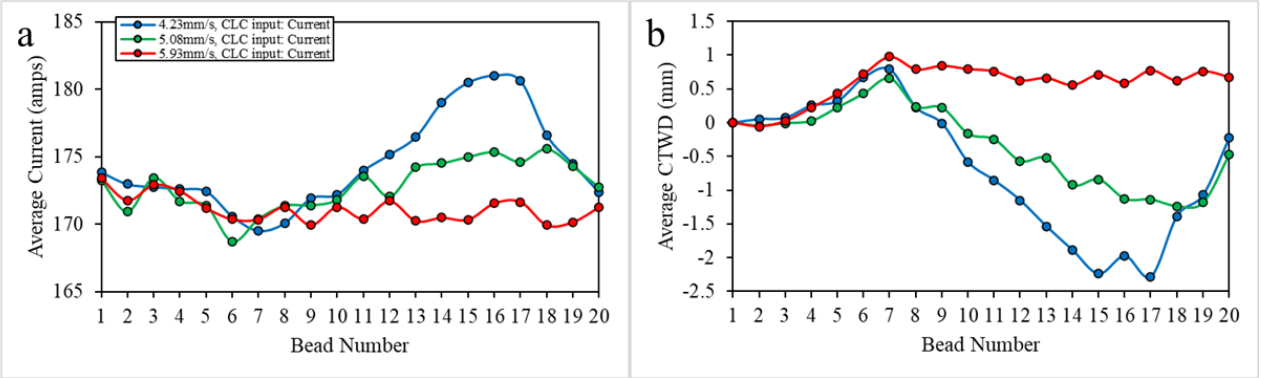

Figure 12: Bead average values for current CUSUM input; a) current, b) CTWD

It can be seen from the CUSUM control charts in Figure 10 and the graphs of control actions in Figure 11 above that while the use of the lowest TS_{OB} = 4.23 mm/s results in 10 layers using 0 s interlayer dwell time, it also results in the widest range of $Sh_{current}$ and $Sl_{current}$ CUSUM values and the widest range of average bead current values. When TS_{OB} = 5.08 mm/s, the range of $Sl_{current}$ CUSUM values stays approximately the same but the $Sh_{current}$ CUSUM values never exceed the control limit. The range of bead average current values decreases but only 7 layers use the 0 s interlayer dwell time. When TS_{OB} = 5.93 mm/s the $Sh_{current}$ CUSUM value again never exceeds the given control limit but the $Sl_{current}$ CUSUM value exceeds the control limit for the majority of the build which causes only the first 5 layers to use the 0 s interlayer dwell time. It should be noted that the range of average layer CTWD values decreases as the value of TS_{OB} increases, mirroring the trend of the average layer current value ranges.

A more succinct way of evaluating the performance of the CUSUM statistical process control method can be achieved by comparing the mean and standard deviation of the in-situ process data for the entirety of each build. The mean and standard deviation of the CTWD and current data for each of the experiments described in Table 3 is shown in Figure 13a and Figure 13b, where the means are given relative to the mean of the reference layer. Thus, an ideal process would have a mean and standard deviation of 0. When TS_{OB} = 4.23 mm/s and the CTWD is used as the input to the CUSUM control process, the ΔCTWD mean is -0.01 mm with a standard deviation of 0.57 mm and the Δ current mean is -2.77 amps with a standard deviation of 2.68 amps. But when TS_{OB} = 4.23 mm/s and the current is used as the input to the CUSUM control process, the ΔCTWD mean is -0.65 mm with a standard deviation of 0.99 mm and the Δ current mean is -0.11 amps with a standard deviation of 4.06 amps. Thus, using the CTWD input allowed for greater control of both CTWD and current. This trend can also be seen to a lesser degree in the experiments where TS_{OB} = 5.08 mm/s. Using CTWD input resulted in a ΔCTWD mean of 0.06 mm with a 0.4 mm standard deviation and a Δ current mean of -3.9 amps with a 2.67 amp standard deviation, but using current input resulted in a ΔCTWD mean of -0.35 mm with a 0.58 mm standard deviation and a Δ current mean of -1.19 amps with a 2.49 amp standard deviation. For the case where TS_{OB} = 5.93 mm/s, the CTWD input experiment yielded a ΔCTWD mean of 0.45 mm with a 0.24 mm standard deviation and a Δ current mean of -1.6 amps with a 2.48 amp standard deviation. The current input experiment resulted in a ΔCTWD mean of 0.81 mm with a 0.35 mm standard deviation and a Δ current mean of -3.06 amps with a 1.97 amp standard deviation. Thus, in the TS_{OB} = 5.93 mm/s experiments selecting one type of input to the CUSUM control chart does not influence the stability of the other data stream like it does in the case where TS_{OB} = 4.23 mm/s.

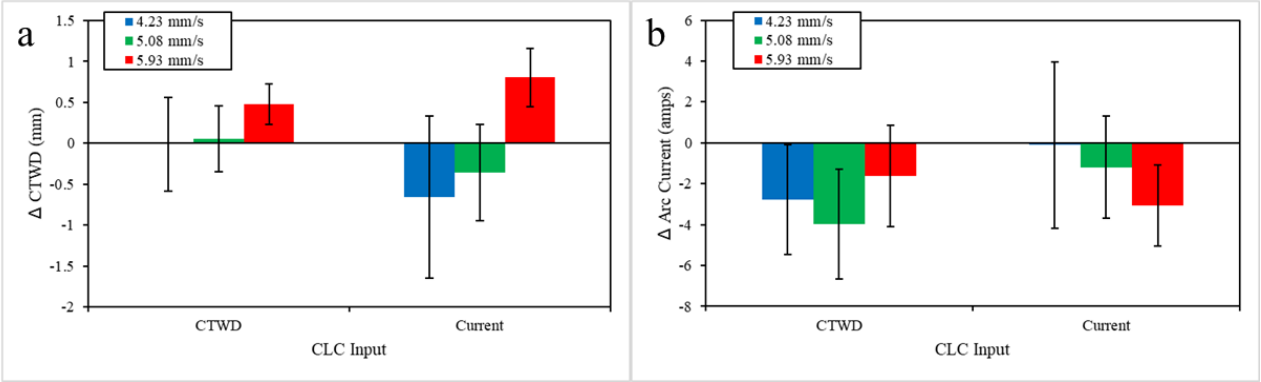

Figure 13: Average values over entire build for each CUSUM input; a) current, b) CTWD

The geometry of the as-deposited parts can be seen below in Figure 14 where the part height and maximum part width are shown. For the CTWD input experiments, the average part height is approximately 41.25 mm with 0.25 mm standard deviation. The average part heights for the current input experiments range from approximately 40.3 to 41.5 mm with a maximum 0.6 mm standard deviation. The expected part height based on the programmed layer height from Table 1 is 40.6 mm so only the TS_{OB} = 5.93 mm/s experiment using current input resulted in an underbuilt part although it is only underbuilt by 0.3 mm. The maximum part widths of the different experiments vary considerably depending on the TS_{OB} value used. When TS_{OB} = 4.23 mm/s, the material input rate is the highest and so naturally those parts have the largest maximum part width

of 10.5-11.5 mm. When the TS_{OB} increases to 5.08 and 5.93 mm/s, thereby decreasing the material input rate, the maximum part also decreases to 8.5-9.5 mm on average. The part widths for the experiments range from approximately 8.5-11.5 mm which fits within previously reported single bead width values of ~3-11 mm by Ding et al. [34] and bulk part width ranges from 8-11 mm in previous work by Thien et al. [8] a variety of deposition process parameters. Additionally, other studies in controlling bead width reported being capable of controlling bead width between 6-9 mm for Xiong et al. [15] and 7-12 mm for Xia et al. [18]. Therefore, even though bead width control is not the focus of the closed loop control method used in this study the resulting variations in part width are comparable to previous efforts.

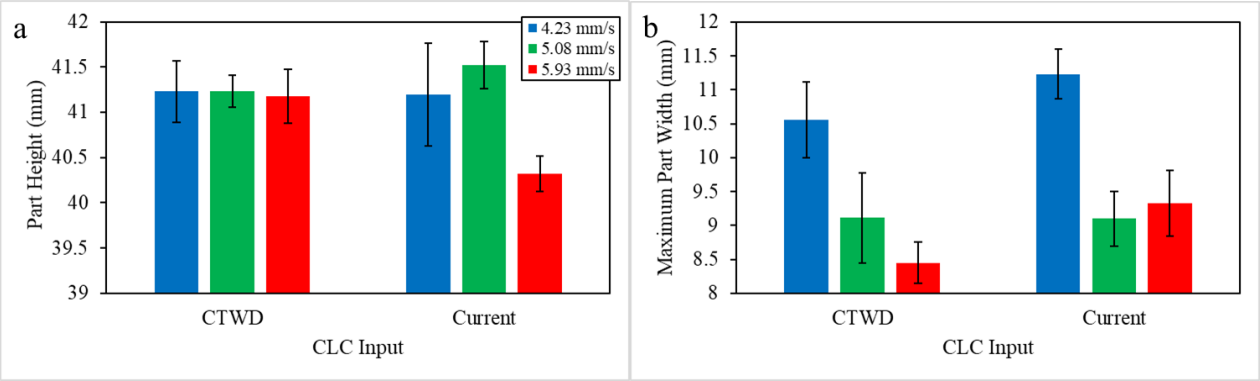

Figure 14: As-deposited part geometry; a) height, b) maximum width

A more comprehensive look at the part geometry can be seen in Figure 15 and Figure 16 below where the average cross-section profile of each part can be seen. When TS_{OB} = 4.23 mm/s the cross-section profile can be seen to have considerable variation in the part width. For the CTWD input experiment the width ranges from approximately 8 mm at the bottom of the part to 10 mm at the widest point halfway up the height of the part at around 20 mm, and for the current input experiment, width ranges from approximately 8 mm at the bottom of the part to 11 mm at the widest point at around 30 mm in height. This variation can be explained by the presence of multiple regions of overbuilding and underbuilding. For the TS_{OB} = 5.08 mm/s experiments, the part width shows less variation but exhibits localized width increases of approximately 9mm an approximate height of 22.5 mm for the CTWD input case and the part width shows less variation but exhibits a gradual increase in part width from approximately 7 mm at the base to around 9mm at a part height of 37 mm for the current input case. When TS_{OB} = 5.93 mm/s, the CTWD input and current input experiments showed the least variation in part width having a small, localized increase in part width from a height of 5 to 10 mm but remaining relatively constant at a width of 8 mm for the remainder of the part. This can be attributed to the fact that for the majority of those depositions, the overbuilding compensation process parameter set is used which stabilizes the resulting geometry.

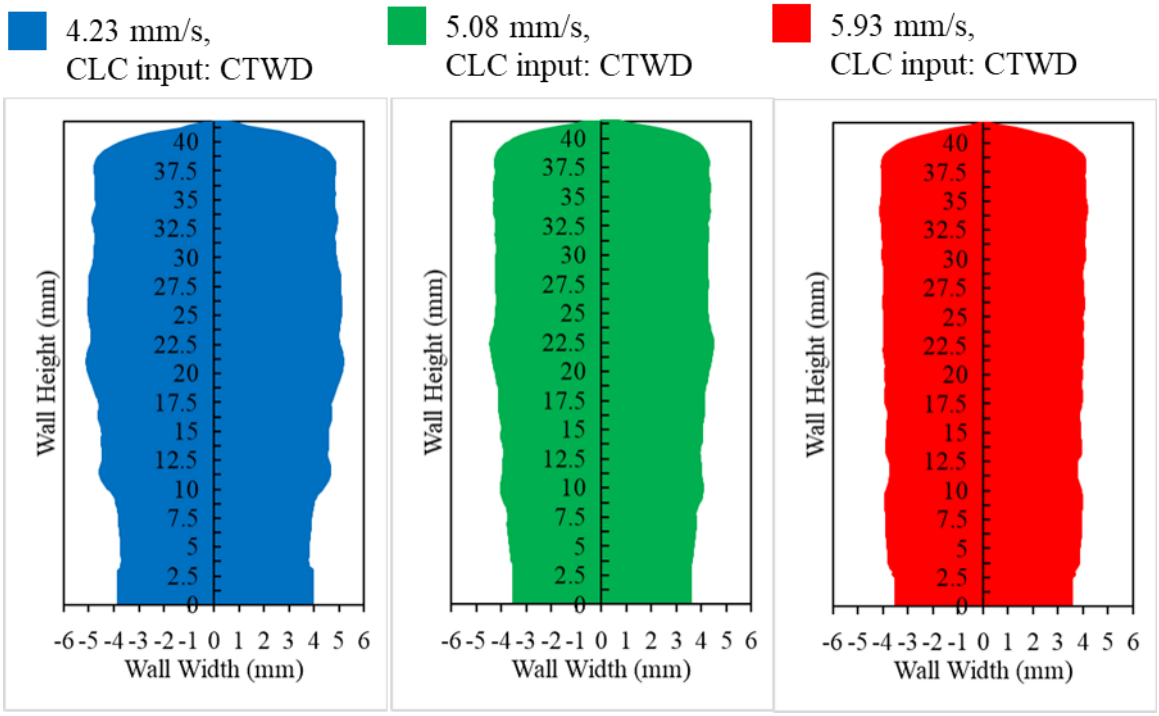

Figure 15: Part geometry cross-section profile for CTWD CUSUM input

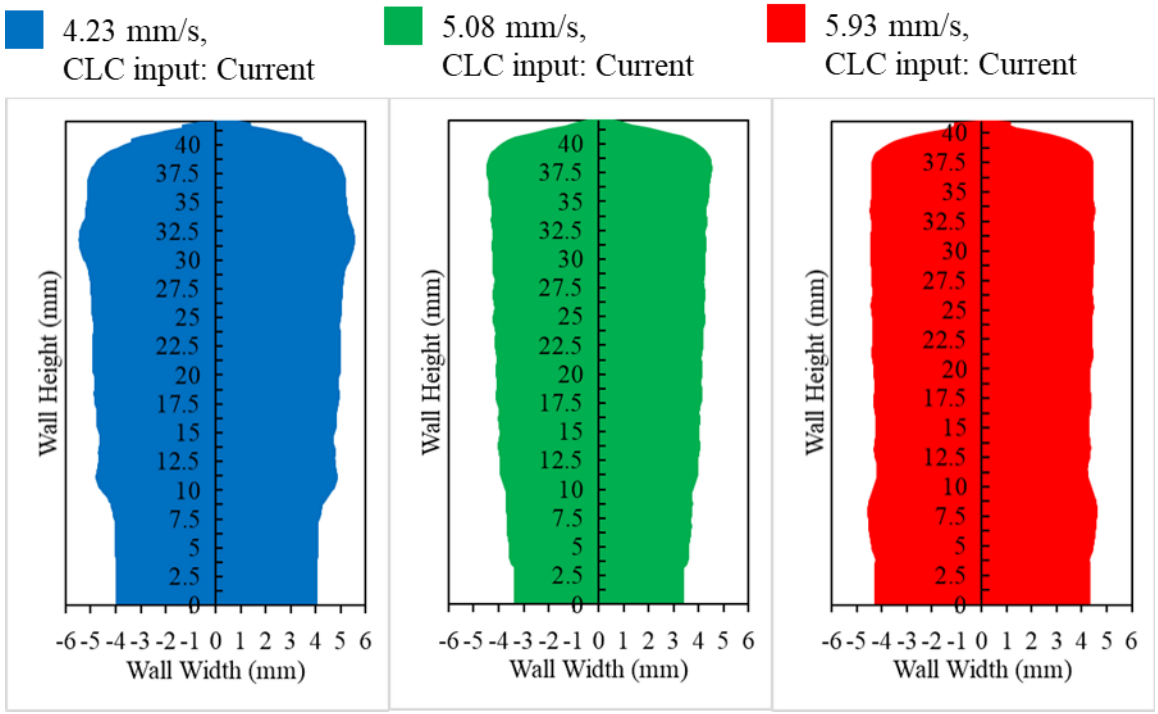

Figure 16: Part geometry cross-section profile for current CUSUM input

Lastly, the influence of closed-loop control strategy on production metrics must be analyzed. The key production metrics evaluated are the deposition time and the material waste, which is denoted here as the buy-to-fly ratio. The deposition times for each experiment can be seen

in Figure 17 below. Overall, the deposition times are dominated by the interlayer dwell time and thus the changes in TS_{OB} do not impact the resulting deposition time very much. The experiments where TS_{OB} = 4.23 mm/s yielded the fastest deposition times of 1300 and 1340 seconds for the CTWD and current input cases, respectively. This is to be expected since those experiments had the greatest number of layers that used the 0 s interlayer dwell time. When TS_{OB} = 5.08 mm/s, the deposition times increased for the CTWD and current input cases to 1380 and 1487 seconds, respectively. Lastly, the deposition where TS_{OB} = 5.93 mm/s have the highest production times of 1505 seconds due to the fact that the majority of the layers in those builds used the overbuilding compensation $T_{D,OB}$ = 60 s.

For the BTF metric trends seen in Figure 18 below, a target geometry must first be established since the BTF ratio is the ratio of deposited volume to desired volume of material. Since the target part height is already given in Table 1 above, the target part width is set as multiple values of 3, 4, and 5 mm to assess how changes in target part width affect BTF. The BTF trends for the CTWD and current input experiments are very similar. In general, the BTF value decreases as the target part width increases, which is to be expected since there is less material to remove. The TS_{OB} = 4.23 mm/s experiments have higher BTF values than those of the TS_{OB} = 5.08 mm/s and TS_{OB} = 5.93 mm/s experiments due to the larger part maximum part widths from the increased material input rate that occurs during the overbuilding compensation portions of those depositions. For the other experiments where TS_{OB} = 5.08 mm/s and TS_{OB} = 5.93 mm/s, the BTF values are very similar for all target part widths.

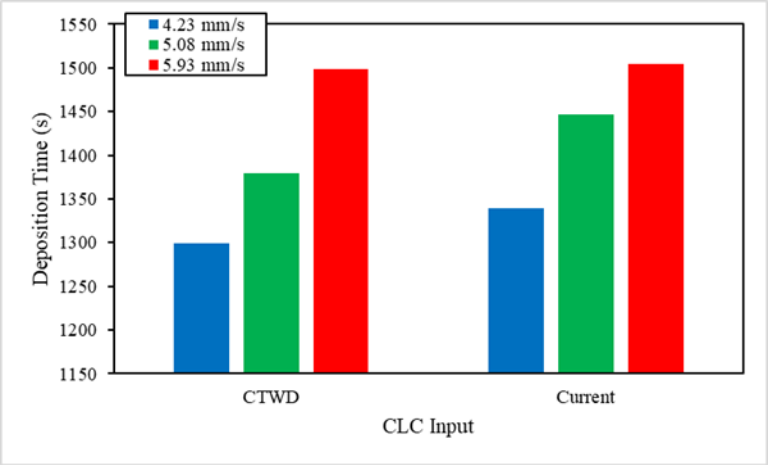

Figure 17: Deposition times

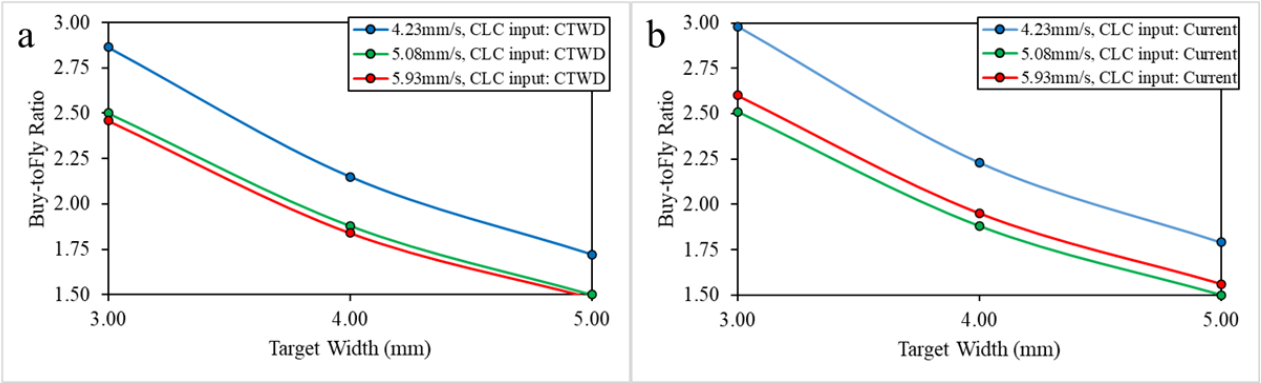

Figure 18: Buy-to-fly ratios for various target part widths; a) CTWD CUSUM input, b) current CUSUM input

The performance of the CUSUM on-off controller utilized in this work can be benchmarked against studies that have applied CUSUM to traditional welding and those that have applied other control techniques to the WAAM process. In the studies by Adolfsson et al. [25,26] and Bevans et al. [28], the goal of the CUSUM technique is to detect intralayer flaws due to substrate defects or introduction of contaminants into the weld pool, and as such the in-situ process data is collected at a much higher frequency (~8-30 kHz) than what is used in this study (5-10 Hz). This allows for flaws to be detected extremely quickly, whereas in the present study the CUSUM alarms for underbuilding are not triggered until ~5 layers after the underbuilding parameters are applied and the overbuilding CUSUM alarm is not triggered until ~4 layers after the overbuilding parameters are applied. In the study by Cowan et al. [33] where "on-off" CUSUM control is used in a grinding process that produced discrete parts, deviations in output parts due to grinding wheel wear are detected and compensated for with a similar lag seen in the results of the present work (exact lag times were not reported in the Cowan et al. [33] study). When compared to the studies that utilized other methods of controlling part height, it must be noted that there are significant differences in material, deposition rate, number of layers deposited, and part geometry that can contribute to the overall efficacy of the height control method. Heralic et al. [13], who utilized both Z position and wire feed speed as control inputs, reported a maximum height deviation of <0.4 mm for a 10-layer deposition using titanium. Li et al. [21], who altered voltage, wire feed speed, and traverse speed, for multi-bead multi-layer depositions, achieved a maximum error of 0.2 mm in part height. Scetinec et al. [17], who continuously updated the Z offset position to compensate for height errors, used current as the in-situ monitoring data stream and reported a maximum deviation of 5 amps in the average layer current throughout the deposition process. Comparatively, in the present work, the best results in terms of reducing variations in CTWD and current occur when TS_{OB} = 5.93 mm/s and CTWD CUSUM is used, where the CTWD ranges from -0.18 to 0.7mm, the current ranges from 170 to 176 amps, and the deposition time is ~1500 s. The trial that results in the lowest deposition time of ~1300 s utilized a low TS_{OB} = 4.23 mm/s, with the CTWD ranging from approximately -1 to 1 mm and the current ranging from approximately 167 to 175 amps. While these results indicate that the CUSUM control method used in this study performs worse than other control methods in terms of managing variations in CTWD and current,

those other studies did not construct their close loop control techniques with production time minimization in mind.

Conclusion

Wire arc additive manufacturing has great potential to fabricate large scale components, but the typically long interlayer dwell times needed for proper thermal management to create more uniform geometry and process conditions are a barrier to larger scale adoption of the process. This study presents a closed-loop control methodology whereby CUSUM statistical process control is used to determine when to apply corrective process parameters to reduce process condition instability caused by using shorter interlayer dwell times. The effect of corrective process parameter magnitude and CUSUM algorithm data input type on controller performance, process variation, and production metrics is studied:

- The CUSUM controller overshoot error for underbuilding is independent of input data type when TS_{OB} = 4.23 mm/s, but when TS_{OB} = 5.08 mm/s the magnitude of the underbuilding overshoot error for CTWD input is roughly half that of the overshoot error when current is the input data type. The number of layers needed for the CUSUM controller to correct the errors induced from underbuilding when current is the input data type is double the number of layers needed when CTWD is the input data type.
- The CUSUM controller overbuilding overshoot error for CTWD input is approximately three times as large as the overbuilding overshoot error for current input when TS_{OB} = 4.23 mm/s. When TS_{OB} = 5.08 mm/s and CTWD input is used, the overbuilding overshoot error decreases considerably. For CTWD input, when TS_{OB} = 4.23 mm/s the number of layers needed to correct the overbuilding error is greater than when TS_{OB} = 4.23 mm/s.
- When TS_{OB} = 5.93 mm/s, there is only underbuilding error in the CUSUM control chart that is never corrected. Thus, the higher TS_{OB} is ineffective at compensating for the underbuilding error.
- The variations in in-situ process data can be described as a series of tradeoffs between process mean and standard deviation. For TS_{OB} = 4.23 mm/s, using CTWD input allows for a better CTWD mean and a worse current mean but also reduces the standard deviation of both the CTWD and the current, whereas using current input yields a better current mean than CTWD but allows for much larger standard deviation in both process data streams. This behavior is also seen when TS_{OB} = 5.08 mm/s albeit to a lesser degree. For TS_{OB} = 5.93 mm/s, there is worse control over the CTWD and current means regardless of data input type, but smaller standard deviations in both data streams can be achieved.
- The trends in production metrics of deposition time and BTF ratio found in this study are largely dependent on the choice of TS_{OB}. The lower the TS_{OB} value, the lower the deposition time but the higher the BTF ratio.

References

[1] T.A. Rodrigues, V. Duarte, R.M. Miranda, T.G. Santos, J.P. Oliveira, Current Status and Perspectives on Wire and Arc Additive Manufacturing (WAAM), Materials. 12 (2019) 1121. https://doi.org/10.3390/ma12071121.

[2] M. Chaturvedi, E. Scutelnicu, C.C. Rusu, L.R. Mistodie, D. Mihailescu, A.V. Subbiah, Wire Arc Additive Manufacturing: Review on Recent Findings and Challenges in Industrial Applications and Materials Characterization, Metals. 11 (2021) 939. https://doi.org/10.3390/met11060939.

[3] Y. Yehorov, L.J. da Silva, A. Scotti, Balancing WAAM Production Costs and Wall Surface Quality through Parameter Selection: A Case Study of an Al-Mg5 Alloy Multilayer-Non-Oscillated Single Pass Wall, JMMP. 3 (2019) 32. https://doi.org/10.3390/jmmp3020032.

[4] J. Xiong, Y. Li, R. Li, Z. Yin, Influences of process parameters on surface roughness of multi-layer single-pass thin-walled parts in GMAW-based additive manufacturing, Journal of Materials Processing Technology. 252 (2018) 128–136. https://doi.org/10.1016/j.jmatprotec.2017.09.020.

[5] H. Geng, J. Li, J. Xiong, X. Lin, D. Huang, F. Zhang, Formation and improvement of surface waviness for additive manufacturing 5A06 aluminium alloy component with GTAW system, RPJ. 24 (2018) 342–350. https://doi.org/10.1108/RPJ-04-2016-0064.

[6] D. Jafari, T.H.J. Vaneker, I. Gibson, Wire and arc additive manufacturing: Opportunities and challenges to control the quality and accuracy of manufactured parts, Materials & Design. 202 (2021) 109471. https://doi.org/10.1016/j.matdes.2021.109471.

[7] F. Li, S. Chen, J. Shi, Y. Zhao, H. Tian, Thermoelectric Cooling-Aided Bead Geometry Regulation in Wire and Arc-Based Additive Manufacturing of Thin-Walled Structures, Applied Sciences. 8 (2018) 207. https://doi.org/10.3390/app8020207.

[8] A. Thien, C. Saldana, T. Kurfess, The effect of WAAM process parameters on process conditions and production metrics in the fabrication of single-pass multi-layer wall artifacts, Int J Adv Manuf Technol. 119 (2022) 531–547. https://doi.org/10.1007/s00170-021-08266-x.

[9] S.H. Lee, Optimization of Cold Metal Transfer-Based Wire Arc Additive Manufacturing Processes Using Gaussian Process Regression, Metals. 10 (2020) 461. https://doi.org/10.3390/met10040461.

[10] F. Li, S. Chen, J. Shi, H. Tian, Y. Zhao, Evaluation and Optimization of a Hybrid Manufacturing Process Combining Wire Arc Additive Manufacturing with Milling for the Fabrication of Stiffened Panels, Applied Sciences. 7 (2017) 1233. https://doi.org/10.3390/app7121233.

[11] J. Karandikar, K. Saleeby, T. Feldhausen, T. Kurfess, T. Schmitz, S. Smith, Evaluation of automated stability testing in machining through closed-loop control and Bayesian machine learning, Mechanical Systems and Signal Processing. 181 (2022) 109531. https://doi.org/10.1016/j.ymssp.2022.109531.

[12] C. Xia, Z. Pan, J. Polden, H. Li, Y. Xu, S. Chen, Y. Zhang, A review on wire arc additive manufacturing: Monitoring, control and a framework of automated system, Journal of Manufacturing Systems. 57 (2020) 31–45. https://doi.org/10.1016/j.jmsy.2020.08.008.

[13] A. Heralić, A.-K. Christiansson, B. Lennartson, Height control of laser metal-wire deposition based on iterative learning control and 3D scanning, Optics and Lasers in Engineering. 50 (2012) 1230–1241. https://doi.org/10.1016/j.optlaseng.2012.03.016.

[14] U. Reisgen, S. Mann, L. Oster, P. Lozano, R. Sharma, Study on Workpiece and Welding Torch Height Control for Polydirectional WAAM by Means of Image Processing, in: 2019

IEEE 15th International Conference on Automation Science and Engineering (CASE), IEEE, Vancouver, BC, Canada, 2019: pp. 6–11. https://doi.org/10.1109/COASE.2019.8843076.
[15] J. Xiong, Z. Yin, W. Zhang, Closed-loop control of variable layer width for thin-walled parts in wire and arc additive manufacturing, Journal of Materials Processing Technology. 233 (2016) 100–106. https://doi.org/10.1016/j.jmatprotec.2016.02.021.
[16] J. Xiong, Y. Zhang, Y. Pi, Control of deposition height in WAAM using visual inspection of previous and current layers, J Intell Manuf. 32 (2021) 2209–2217. https://doi.org/10.1007/s10845-020-01634-6.
[17] A. Ščetinec, D. Klobčar, D. Bračun, In-process path replanning and online layer height control through deposition arc current for gas metal arc based additive manufacturing, Journal of Manufacturing Processes. 64 (2021) 1169–1179. https://doi.org/10.1016/j.jmapro.2021.02.038.
[18] C. Xia, Z. Pan, S. Zhang, H. Li, Y. Xu, S. Chen, Model-free adaptive iterative learning control of melt pool width in wire arc additive manufacturing, Int J Adv Manuf Technol. 110 (2020) 2131–2142. https://doi.org/10.1007/s00170-020-05998-0.
[19] A. Fathi, A. Khajepour, E. Toyserkani, M. Durali, Clad height control in laser solid freeform fabrication using a feedforward PID controller, Int J Adv Manuf Technol. 35 (2007) 280–292. https://doi.org/10.1007/s00170-006-0721-1.
[20] T.F. Lam, Y. Xiong, A.G. Dharmawan, S. Foong, G.S. Soh, Adaptive process control implementation of wire arc additive manufacturing for thin-walled components with overhang features, Int J Adv Manuf Technol. 108 (2020) 1061–1071. https://doi.org/10.1007/s00170-019-04737-4.
[21] Y. Li, X. Li, G. Zhang, I. Horváth, Q. Han, Interlayer closed-loop control of forming geometries for wire and arc additive manufacturing based on fuzzy-logic inference, Journal of Manufacturing Processes. 63 (2021) 35–47. https://doi.org/10.1016/j.jmapro.2020.04.009.
[22] S. Zhang, Process control for WAAM using computer vision, (n.d.) 154.
[23] H. Pham, ed., Springer Handbook of Engineering Statistics, Springer London, London, 2023. https://doi.org/10.1007/978-1-4471-7503-2.
[24] NIST/SEMATECH e-Handbook of Statistical Methods, NIST, 2022. http://www.itl.nist.gov/div898/handbook/.
[25] S. Adolfsson, A. Bahrami, I. Claesson, Quality monitoring in robotised welding using sequential probability ratio test, in: Proceedings of Digital Processing Applications (TENCON '96), IEEE, Perth, WA, Australia, 1996: pp. 635–640. https://doi.org/10.1109/TENCON.1996.608417.
[26] S. Adolfsson, A. Bahrami, G. Bolmsj, On-Line Quality Monitoring in Short-Circuit Gas Metal Arc Welding, (n.d.).
[27] R. Li, J. Li, J. Liu, Body Welding Quality Control Based on a CUSUM Control Chart, AMR. 228–229 (2011) 1080–1084. https://doi.org/10.4028/www.scientific.net/AMR.228-229.1080.
[28] B. Bevans, A. Ramalho, Z. Smoqi, A. Gaikwad, T.G. Santos, P. Rao, J.P. Oliveira, Monitoring and flaw detection during wire-based directed energy deposition using in-situ acoustic sensing and wavelet graph signal analysis, Materials & Design. 225 (2023) 111480. https://doi.org/10.1016/j.matdes.2022.111480.
[29] A. Shah, R. Aliyev, H. Zeidler, S. Krinke, A Review of the Recent Developments and Challenges in Wire Arc Additive Manufacturing (WAAM) Process, JMMP. 7 (2023) 97. https://doi.org/10.3390/jmmp7030097.

[30] M.R. Zahidin, F. Yusof, S.H. Abdul Rashid, S. Mansor, S. Raja, M.F. Jamaludin, Y.Hp. Manurung, M.S. Adenan, N.I. Syahriah Hussein, Research challenges, quality control and monitoring strategy for Wire Arc Additive Manufacturing, Journal of Materials Research and Technology. 24 (2023) 2769–2794. https://doi.org/10.1016/j.jmrt.2023.03.200.
[31] N. Kozamernik, D. Bračun, D. Klobčar, WAAM system with interpass temperature control and forced cooling for near-net-shape printing of small metal components, Int J Adv Manuf Technol. 110 (2020) 1955–1968. https://doi.org/10.1007/s00170-020-05958-8.
[32] S. Banerjee, A new adaptive process control scheme for efficient wire arc additive manufacturing of thin-walled SS308L component, The International Journal of Advanced Manufacturing Technology. (2022) 15.
[33] R.W. Cowan, D.J. Schertz, T.R. Kurfess, An Adaptive Statistically Based Controller for Through-Feed Centerless Grinding, Journal of Manufacturing Science and Engineering. 123 (2001) 380–386. https://doi.org/10.1115/1.1381398.
[34] D. Ding, Z. Pan, D. Cuiuri, H. Li, S. van Duin, N. Larkin, Bead modelling and implementation of adaptive MAT path in wire and arc additive manufacturing, Robotics and Computer-Integrated Manufacturing. 39 (2016) 32–42. https://doi.org/10.1016/j.rcim.2015.12.004.